J|A|C|S
ARTICLES
Published on Web 10/21/2005

Oxoselenido Clusters of the Lanthanides: Rational Introduction of Oxo Ligands and Near-IR Emission from Nd(III)

Santanu Banerjee,[†] Louise Huebner,[†] Michael D. Romanelli,[†] G. Ajith Kumar,[‡] Richard. E. Riman,[‡] Thomas J. Emge,[†] and John G. Brennan*,[†]

Contribution from the Department of Chemistry and Chemical Biology, and Materials Science and Engineering, Rutgers, the State University of New Jersey, 610 Taylor Road, Piscataway, New Jersey 08854-8087

Received June 28, 2005; E-mail: bren@ccbmail.rutgers.edu

Abstract: Reactions of $Ln(SePh)_3$ with SeO_2 in THF give octanuclear oxoselenido clusters with the general formula $(THF)_8Ln_8O_2Se_2(SePh)_{16}$ (Ln = Ce, Pr, Nd, Sm). In this isomorphous series, the eight Ln(III) ions are connected in the center by a pair of μ_3-O^{2-} ligands and μ_5-Se^{2-} ligands, with 14 bridging and two terminal selenolate ligands capping the cluster surface. Thermal decomposition at 700 °C of the Nd compound in vacuo led to the formation of a phase mixture of $NdSe_2$, Nd_2Se_3, and Nd_2O_3. Near-IR emission experiments on the $(THF)_8Nd_8O_2Se_2(SePh)_{16}$ and the fluorinated thiolate compound $(DME)_2Nd(SC_6F_5)_3$ demonstrate that clusters with oxo ligands are not only highly emissive, but also they emit at wavelengths not found in conventional oxides.

Introduction

Emission of light from lanthanide ions is a fundamentally important process with a continuously expanding range of applications in contemporary electronic devices, from TV screens to lasers and optical fibers.[1−5] Control of emission intensity is often elusive, with competitive processes such as upconversion, photon splitting, or nonradiative (vibronic) quenching often detracting from ideal performance.[6] While introduction of Ln into solid-state oxide materials has long been facile, the incorporation of near-IR emissive lanthanide ions into unconventional materials (i.e., organic polymers) remains challenging due to the intrinsic properties of Ln sources and the various technological barriers associated with solids processing.

The utility of solid-state Ln compounds as Ln doping sources is moderated by the insolubility of these materials in apolar matrixes. Molecular Ln sources are soluble, but suffer from the tendency of these compounds to contain ligands with high energy vibrational modes (i.e., ligands with C−H or O−H functional groups) that vibrationally relax emissive states.[7] Further, the voluminous nature of most ligand systems precludes the delivery of high Ln concentrations. Cluster compounds, with their solubility in organic solvents, their relative absence of high-energy vibrational modes, and the relatively high concentration of Ln ions/unit volume, are promising sources of lanthanide ions in the preparation of emissive materials.

In Ln cluster synthesis, addition of E (E = S/Se/Te) to solutions of $Ln(EPh)_3$ has been a reliable synthetic approach to a wealth of compounds with E^{2-} and EE^{2-} ligands, heterometallic and heterochalcogen species.[8−17] Most recently, an Er_{10} cluster with both surface and internal Er atoms was found to exhibit exceptional emission at 1.54 μm.[18] Subsequent studies have revealed that Er cluster compounds can be used to deliver high concentrations of emissive Er ions into apolar matrixes.[19]

Unfortunately, the air sensitivity of Ln_xE_y clusters presents an obstacle in composite materials synthesis. Air stable ligands such as O^{2-} are potentially useful, but the chemistry of lanthanide oxo cluster compounds is complicated by the fact that oxo compounds[20−29] can react with water to form hydroxides.

[†] Department of Chemistry and Chemical Biology.
[‡] Materials Science and Engineering.

(1) Silversmith, A. J.; Lenth, W.; Macfarlane, R. M. *Appl. Phys. Lett*. **1987**, *51*, 1997.
(2) Maciel, G. S.; de Arajuo, C. B.; Massaddeq, Y.; Aegerter, M. A. *Phys. Rev. B* **1997**, *55*, 6335.
(3) Hebert, T.; Wannermacher, R.; Lenth, W.; Macfarlane, R. M. *Appl. Phys. Lett.* **1990**, *57*, 1727.
(4) Dowing, E.; Hesselink, L.; Ralston, J.; Macfarlane, R. M. *Science* **1986**, *273*, 1185.
(5) Bhargava, R. N.; Gallaghar, D.; Hong, X.; Nurmikko, A. *Phys. Rev. Lett.* **1994**, 416.
(6) *Spectroscopy of Solid State Laser Type Materials*; Di Bartolo, B., Ed.; Plenum Press: New York, 1987.
(7) Beeby, A.; Faulkner, S. *Chem. Phys. Lett.* **1997**, *266*, 116.
(8) Freedman, D.; Emge, T. J.; Brennan, J. G. *J. Am. Chem. Soc.* **1997**, *119*, 11112.
(9) Melman, J. H.; Emge, T. J.; Brennan, J. G. *Chem. Commun.* **1997**, 2269.
(10) Melman, J. H.; Emge, T. J.; Brennan, J. G. *Inorg. Chem.* **1999**, *38*, 2117.
(11) Freedman, D.; Emge, T. J.; Brennan, J. G. *Inorg. Chem.* **1999**, *38*, 4400.
(12) Freedman, D.; Melman, J. H.; Emge, T. J.; Brennan, J. G. *Inorg. Chem.* **1998**, *37*, 4162.
(13) Kornienko, A.; Emge, T. J.; Brennan, J. G. *J. Am. Chem. Soc.* **2001**, *123*, 11933.
(14) Fitzgerald, M.; Emge, T. J.; Brennan, J. G. *Inorg. Chem*. **2002**, *41*, 3528.
(15) Freedman, D.; Emge, T. J.; Brennan, J. G. *Inorg. Chem.* **2002**, *41*, 492.
(16) Kornienko, A.; Emge, T. J.; Hall, G.; Brennan, J. G. *Inorg. Chem*. **2002**, *41*, 121.
(17) Huebner, L.; Kornienko, A.; Emge, T. J.; Brennan, J. G. *Inorg. Chem*. **2005**, *44*, 5118.
(18) Kornienko, A.; Kumar, G. A.; Riman, R. E.; Emge, T. J.; Brennan, J. G. *J. Am. Chem. Soc*. **2005**, *127*, 3501.
(19) Kumar, A.; Riman, R.; Chen, S.; Smith, D.; Ballato, J.; Banerjee, S.; Kornienko, A.; Brennan, J. *Appl. Phys. Lett.*, submitted.
(20) Liu, J.; Meyers, E. A.; Shore, S. G. *Inorg. Chem.* **1998**, *37*, 5410.

10.1021/ja054261q CCC: $30.25

Oxo compounds without OH ligands are rare, often isolated from reactions of air-sensitive Ln complexes with "adventitious" water. More recently, an elegant series of oxo clusters have been prepared in aqueous environments.[30−33] In these aqueous preparations, aqua and hydroxide ligands are also present in the products, and such functional groups unfortunately quench low energy emissions. Methods for introducing oxo ligands that do not concomitantly afford the possibility of introducing OH/OH_2 ligands are essentially nonexistent.

Of the technologically important near-IR emission sources, Nd, Tm, and Er stand out. The emission of Er at 1.54 μm is used extensively in telecommunications because glass fibers are transparent to this wavelength.[34] Both Tm and Nd are alluring additions to optical fiber manufacture because they can effectively broaden the available bandwidth that can be amplified optically. Nd is the more complicated emission source of the three, with a cascade of emission energies[6,35] that are either rarely (1.34 μm) or never (1.81 μm) observed either from molecular Nd sources or from metal oxides.[36] Of these transitions, 1.34 μm is relevant to the telecommunications window. Chemical modification intended to enhance Nd emission, such as Nd to fluorescein,[37] porphyrin,[38] or terphenyl[39] sensitizers, remains a challenging synthetic goal.

In the obvious extension of chalcogenido cluster chemistry to oxo systems, reactions of $Ln(EPh)_3$ with elemental oxygen have yet to give crystalline oxo products in any significant yield. In this work, we demonstrate the utility of SeO_2 as an alternative, soluble source of oxo ligands, in reactions with $Ln(SePh)_3$ that give a homologous series of crystalline oxoselenido cluster compounds. The thermolysis chemistry of these clusters has been investigated, and the near-IR emission properties of the Nd cluster compound are reported and compared to the novel molecular fluorothiolate $(DME)_2Nd(SC_6F_5)_3$.

Experimental Section

General Methods. All syntheses were carried out under high purity nitrogen (WELCO Praxair), using conventional drybox or Schlenk techniques. Solvents (Aldrich) were purified with a dual column Solv-Tek Solvent Purification System. Lanthanides, SeO_2, and Hg were purchased from Strem. HSC_6F_5 was purchased from Aldrich. PhSeSePh was purchased from Aldrich and recrystallized from hexane. $Hg(SC_6F_5)_2$ was prepared according to the literature procedure.[40] Melting points were taken in sealed capillaries and are uncorrected. IR spectra were taken on a Thermo Nicolet Avatar 360 FTIR spectrometer and were recorded from 4000 to 600 cm^{-1} as a Nujol mull on NaCl plates. Electronic spectra were recorded on a Varian DMS 100S spectrometer with the samples in a 0.10 mm quartz cell attached to a Teflon stopcock. Powder diffraction spectra were obtained from Bruker AXS D8 Advance diffractometer using Cu Kα radiation. Elemental analyses were performed by Quantitative Technologies, Inc. (Whitehouse Station, NJ). The compounds are air-sensitive and are particularly unstable when isolated from the mother liquor. They appear to lose lattice solvent more rapidly than anything we have yet encountered, to the extent that mounting crystals for diffraction analysis by our conventional methods was impossible for the Sm compound.

Synthesis of $(THF)_8Ce_8(\mu_3\text{-}O)_2(\mu_5\text{-}Se)_2(SePh)_{16}\cdot 6THF$ (1). Ce (0.140 g, 1.0 mmol), PhSeSePh (0.47 g, 1.5 mmol), and Hg (0.024 g, 0.11 mmol) were combined in THF (ca. 30 mL), and the mixture was stirred until all of the metal was consumed (1 day) to give a yellow solution with a small amount of greenish-yellow solid at the bottom of the flask. The solution was filtered, and SeO_2 (0.11 g, 1.0 mmol) was added to the filtrate. The resulting mixture was stirred for 1 h at 55 °C, during which the SeO_2 dissolved to give a brownish-yellow solution that was filtered, reduced in volume under vacuum to ca. 15 mL, and layered with hexane (15 mL) to give yellow plate-shaped crystals (0.33 g, 68%) that turn yellow-brown between 75 and 80 °C, darken between 100 and 150 °C, melt at 180 °C, and remain dark brown from 200 to 350 °C. IR: 3043 (m), 2967 (s), 2943 (s), 2914 (s), 2728 (w), 1567 (m), 1468 (s), 1374 (m), 1293 (w), 1246 (w), 1170 (w), 1071 (m), 1018 (m), 901 (w), 727 (m), 680 (w) cm^{-1}. UV−vis: no well-defined absorption maximum was observed from 300 to 750 nm when the compound was dissolved in pyridine. Anal. Calcd for $C_{152}H_{192}Ce_8O_{16}Se_{18}$: C, 37.9; H, 4.02. Found: C, 35.7; H, 3.36.

Synthesis of $(THF)_8Pr_8(\mu_3\text{-}O)_2(\mu_5\text{-}Se)_2(SePh)_{16}\cdot 6THF$ (2). As for **1**, Pr (0.14 g, 1.0 mmol), PhSeSePh (0.47 g, 1.5 mmol), and Hg (0.024 g, 0.11 mmol) in THF (ca. 30 mL) gave an olive-green solution with a small amount of green solid that was removed by filtration. SeO_2 (0.110 g, 1 mmol) was added to the filtrate, the resulting mixture was stirred for 1 h at 55 °C, after which all of the SeO_2 was dissolved. The lime-green solution was filtered and reduced in volume under vacuum to ca. 15 mL, and layered with hexane (15 mL) to give green rod-shaped crystals after 2 days (0.35 g, 64%) that turn light brown between 75 and 80 °C, darken between 120 and 150 °C, melt at 185 °C, and remain dark brown from 200 to 350 °C. IR: 3043 (m), 2956 (s), 2926 (s), 2722 (w), 1567 (m), 1444 (m), 1374 (m), 1293 (w), 1252 (w), 1176 (w), 1071 (m), 1024 (m), 908 (w), 733 (w), 680 (w) cm^{-1}. UV−vis: The compound does not display absorption maximum from 300 to 750 nm when dissolved in pyridine. Anal. Calcd for $C_{152}H_{192}Pr_8O_{16}Se_{18}$: C, 37.8; H, 4.01. Found: C, 37.1; H, 3.16.

Synthesis of $(THF)_8Nd_8(\mu_3\text{-}O)_2(\mu_5\text{-}Se)_2(SePh)_{16}\cdot 6THF$ (3). As with **2**, Nd (0.144 g, 1.0 mmol), PhSeSePh (0.468 g, 1.5 mmol), and Hg (0.024 g, 0.11 mmol) in THF (ca. 30 mL) gave a blue-colored solution with a small amount of pale blue solid. The solution was filtered, SeO_2 (0.110 g, 1 mmol) was added, the mixture was filtered, reduced in volume under vacuum to ca. 15 mL, and layered with hexane (15 mL) to give blue rod-shaped crystals after 2 days (0.41 g, 69%) that turn light brown between 75 and 80 °C, darken between 120 and 150 °C, melt at 185 °C, and remain dark brown from 200 to 350 °C. IR: 3043

(21) Hubert-Pfalzgraf, L. G.; Miele-Pajot, N.; Papiernik, R.; Vaissermann, J. *J. Chem. Soc., Dalton Trans.: Inorg. Chem.* **1999**, 4127.
(22) Ma, B.; Gao, S.; Bai, O.; Sun, H.; Xu, G. *J. Chem. Soc., Dalton Trans.* **2000**, 1003.
(23) Kritikos, M.; Moustiakimov, M.; Wijk, M.; Westin, G. *J. Chem. Soc., Dalton Trans.* **2001**, 1931.
(24) Tasiopoulos, A. J.; O'Brien, T.; Abboud, K. A.; Christou, G. *Angew. Chem., Int. Ed.* **2004**, *43*, 345.
(25) Xu, G.; Wang, Z.; He, Z.; Lue, Z.; Liao, C.; Yan, C. *Inorg. Chem.* **2002**, *41*, 6802.
(26) Schuetz, S. A.; Silvernail, C. M.; Incarvito, C. D.; Rheingold, A. L.; Clark, J. L.; Day, V. W.; Belot, J. A. *Inorg. Chem.* **2004**, *43*, 6203.
(27) Anwander, R.; Munck, F. C.; Priermeier, T.; Scherer, W.; Runte, O.; Herrmann, W. A. *Inorg. Chem.* **1997**, *36*, 3545.
(28) Pernin, C. G.; Ibers, J. A. *Inorg. Chem.* **1997**, *36*, 3802.
(29) Wai-H. Lam, A.; Wong, W.; Wen, G.; Zhang, X.; Gao, S. *New J. Chem.* **2001**, *25*, 531.
(30) Wang, R.; Selby, H. D.; Liu, H.; Carducci, M. D.; Jin, T.; Zheng, Z.; Anthis, J. W.; Staples, R. J. *Inorg. Chem.* **2002**, *41*, 278.
(31) Zhang, D.; Ma, B.; Jin, T.; Gao, S.; Yan, C.; Mak, T. C. W. *New J. Chem.* **2000**, *24*, 61.
(32) Wang, R.; Carducci, M. D.; Zheng, Z. *Inorg. Chem.* **2000**, *39*, 1836.
(33) Zhang, M.; Zhang, J.; Zheng, S.; Yang, G. *Angew. Chem., Int. Ed.* **2005**, *44*, 1385.
(34) Becker, P. C.; Olsson, N. A.; Simpson, J. R. *Erbium doped fiber amplifiers-Fundamentals and Technology*; Academic Press: New York, 1999.
(35) Kaminski, A. A. *Laser Crystals-Their Physics and Properties*; Springer: Berlin, 1989.
(36) Kaminski, A. A. *Crystalline Lasers-Physical Processes and Operating Scheme*; CRC Press: New York, 1996.
(37) Wolbers, M. P. O.; Van Veggel, F. C. J. M.; Peters, F. G. A.; Van Beelen, E. S. E.; Hofstraat, J. W.; Geurts, F. A. J.; Reinhoudt, D. N. *Chem.-Eur. J.* **1998**, *4*, 772.
(38) Beeby, A.; Dickins, R. S.; FitzGerald, S.; Govenlock, L. J.; Parker, D.; Williams, J. A. G.; Maupin, C. L.; Riehl, J. P.; Siligardi, G. *Chem. Commun.* **2000**, 1183.
(39) Wolbers, M. P. O.; Van Veggel, F. C. J. M.; Snellink-Ruel, B. H. M.; Hofstraat, J. W.; Guerts, F. A. J.; Reinhoudt, D. N. *J. Chem. Soc., Perkin Trans. 2* **1998**, 2141.
(40) Peach, M. E. *J. Inorg. Nucl. Chem.* **1973**, *35*, 1046.

Table 1. Summary of Crystallographic Details for **1**−**4**

	compound			
	1	**2**	**3**	**4**
empirical formula	$C_{149}H_{186}O_{15.25}Ce_8Se_{18}$	$C_{149}H_{186}O_{15.25}Pr_8Se_{18}$	$C_{152}H_{192}O_{16}Nd_8Se_{18}$	$C_{141}H_{170}O_{13.25}Sm_8Se_{18}$
fw	4763.22	4768.74	4850.26	4699.05
space group	*P*2(1)/*c*	*P*2(1)/*c*	*P*2(1)/*c*	*P*2(1)/*n*
a (Å)	16.804(2)	16.803(2)	17.126(1)	17.833(6)
b (Å)	16.718(2)	16.732(2)	16.941(1)	21.011(7)
c (Å)	29.929(3)	28.875(3)	28.758(2)	22.611(8)
β (deg)	91.455(2)	91.403(2)	91.299(1)	102.181(6)
V (Å^3)	8124(2)	8116(1)	8341(1)	8304(5)
Z	2	2	2	2
D(calcd) (g/cm^{-3})	1.947	1.951	1.931	1.879
temp (°C)	−173	−173	−73	20
λ (Å)	0.71073	0.71073	0.71073	0.71073
abs coeff (mm^{-1})	6.280	6.444	6.425	6.776
$R(F)^a$ [$I > 2\sigma(I)$]	0.0448	0.0389	0.0404	0.0385
$R_w(F^2)^a$ [$I > 2\sigma(I)$]	0.1150	0.0913	0.0926	0.0958

[a] $R(F) = \sum||F_o| - |F_c||/\sum|F_o|$; $R_w(F^2) = \{\sum[w(F_o^2 - F_c^2)^2]/\sum[w(F_o^2)^2]\}^{1/2}$. Additional crystallographic details are given in the Supporting Information.

(m), 2955 (s), 2920 (s), 2716 (w), 1567 (w), 1444 (m), 1374 (m), 1287 (w), 1246 (w), 1153 (w), 1059 (w), 1012 (w), 728 (m), 680 (w) cm^{-1}. Anal. Calcd for $C_{144}H_{176}Nd_8O_{14}Se_{18}$: C, 36.7; H, 3.77. Found: C, 36.1; H, 3.60. The compound also crystallizes as found for the Sm cluster **4**: X-ray diffraction; unit cell *P*2(1)/*n*, with $a = 17.869(4)$ Å, $b = 20.734(4)$ Å, $c = 22.661(4)$ Å, $\beta = 101.67(4)°$, $V = 8222(1)$ Å^3 at −120 °C.

Synthesis of (THF)$_8$Sm$_8$(μ_3-O)$_2$(μ_5-Se)$_2$(SePh)$_{16}$·4THF (4). Method A: Sm (0.150 g, 1.0 mmol), PhSeSePh (0.468 g, 1.5 mmol), and Hg (0.024 g, 0.11 mmol) were combined in THF (ca. 30 mL), and the mixture was stirred until all of the metal was consumed (2 days) to give a yellow-orange solution with a small amount of yellow-orange solid. The solution was filtered, and SeO_2 (0.110 g, 1 mmol) was added to the filtrate. The resulting mixture was stirred for 1 h at 55 °C to give an orange-colored solution that was filtered, reduced in volume to ca. 15 mL, and layered with hexane (15 mL) to give yellow-orange plate-shaped crystals (0.27 g, 59%). Method B: Sm (0.40 g, 2.7 mmol), PhSeSePh (1.25 g, 4.0 mmol), and Hg (0.029 g, 0.12 mmol) were combined in THF (ca. 45 mL), and the mixture was stirred for 1 day until all of the metal was consumed to give an orange-colored solution. SeO_2 (0.11 g, 1.0 mmol) was added to the solution. The resulting mixture was stirred for 2 days at room temperature, giving an orange-colored solution. The solution was allowed to settle for a few days whence some gray precipitate appeared. The solution was filtered (42 mL) and layered with hexane (43 mL) to give yellow-orange plate-shaped crystals after 2 days (0.98 g, 62%). These crystals turn a red-orange color between 75 and 80 °C, darken around 130 °C, melt between 170 and 190 °C, and turn dark brown from 275 to 350 °C. IR: 2924 (s), 2726 (w), 1573 (w), 1460 (m), 1377 (m), 1295 (w), 1260 (m), 1094 (w), 1068 (w), 1020 (m), 732 (m), 690 (w), 666 (w) cm^{-1}. UV−vis: There was no resolved LMCT absorption maximum from 300 to 750 nm when dissolved in pyridine. Anal. Calcd for $C_{144}H_{176}Sm_8O_{14}Se_{18}$: C, 36.4; H, 3.73. Found: C, 35.1; H, 3.40.

Synthesis of (DME)$_2$Nd(SC$_6$F$_5$)$_3$ (5). Nd (0.14 g, 1.0 mmol) and $Hg(SC_6F_5)_2$ (0.90 g, 1.5 mmol) were combined in DME (ca. 20 mL), and the mixture was stirred overnight until the metal flakes were completely consumed and elemental mercury was visible in the bottom of the flask. The pale blue/green solution was filtered away from the mercury (0.25 g, 82%), and layered with hexane (ca. 20 mL) to give near colorless pale blue crystals (0.92 g, 96%) that turn red at 140 °C and melt at 145 °C. IR: 2949 (s), 2926 (s), 2844 (s), 2725 (w), 2394 (w), 2345 (w), 1883 (w), 1707 (w), 1619 (m), 1568 (w), 1508 (s), 1461 (s), 1380 (s), 1257 (m), 1187 (w), 1082 (m), 1030 (s), 960 (s), 866 (s), 721 (w) cm^{-1}. Anal. Calcd for $C_{26}H_{20}F_{15}NdO_4S_3$: C, 33.9; H, 2.20. Found: C, 34.7; H, 2.55. X-ray diffraction: unit cell $P\bar{1}$, with $a = 8.5954(5)$ Å, $b = 12.7731(7)$ Å, $c = 15.2844(9)$ Å, $\alpha = 71.244(1)°$, $\beta = 84.394(1)°$, $\gamma = 88.361(1)°$, $V = 1581(2)$ Å^3, $Z = 2$. The compound is structurally similar to an earlier reported Er derivative.[41]

Thermolysis and X-ray Powder Diffraction Measurements. A sample of **3** was placed in a quartz tube that was then sealed under vacuum. The end of the tube with the sample was placed in an oven, and the temperature was raised (20 °C/min) to 650 °C, and held at this temperature for 5 h. The other end of the thermolysis tube was kept in liquid nitrogen during the experiment. Black powder formed, and an X-ray powder diffraction pattern was obtained by scanning from 20 to 80 °C. The colorless liquid that condensed in the cold part of the tube was dissolved in acetonitrile and analyzed by GC/MS.

X-ray Structure Determination of 1−4. Data for **1**−**4** were collected on a Bruker Smart APEX CCD diffractometer with graphite monochromatized Mo Kα radiation ($\lambda = 0.71073$ Å) at 100 K. Crystals of **1**−**3** were immersed in Paratone oil and examined at low temperatures, whereas **4** lost solvent too quickly for this procedure, and a crystal of **4** had to be mounted in a glass capillary along with THF. The data were corrected for Lorenz effects and polarization, and absorption, the latter by a multiscan (SADABS)[42] method. The structures were solved by Patterson or direct methods (SHELXS86).[43] All non-hydrogen atoms were refined (SHELXL97)[44]based upon F_{obs}^2. All hydrogen atom coordinates were calculated with idealized geometries (SHELXL97). Scattering factors (f_o, f', f'') are as described in SHELXL97. Crystallographic data and final *R* indices for **1**−**4** are given in Table 1. An ORTEP diagram[45,46] for the isomorphous core of **1**−**4** is shown in Figure 1. Significant bond geometries for **1**−**4** are given in Tables 2 and 3. Complete crystallographic details for **1**−**4** are given in the Supporting Information.

Optical Characterization. Absorption measurements were carried out with compounds dissolved in THF using a double beam spectrophotometer (Perkin-Elmer Lambda 9, Wellesley, MA) in a 1 cm cuvette using THF as the reference solvent at approximately 0.01 M. The emission spectra of the Nd samples were recorded by exciting the sample with the 800 nm band of a laser diode in the 45° excitation geometry. The emission from the sample was focused onto a 1 m monochromator (Jobin Yvon, Triax 550, Edison, NJ) and detected by

(41) Melman, J.; Rhode, C.; Emge, T. J.; Brennan, J. G. *Inorg. Chem*. **2002**, *41*, 28.
(42) Bruker-ASX. *SADABS*, Bruker Nonius area detector scaling and absorption correction, v2.05; Bruker-AXS Inc.: Madison, WI, 2003.
(43) Sheldrick, G. M. *SHELXS86*, Program for the Solution of Crystal Structures; University of Göttingen: Germany, 1986.
(44) Sheldrick, G. M. *SHELXL97*, Program for Crystal Structure Refinement; University of Göttingen: Germany, 1997.
(45) Johnson, C. K. ORTEP II, Report ORNL-5138; Oak Ridge National Laboratory, Oak Ridge, TN, 1976.
(46) Sheldrick, G. M. *SHELXTL* (XP). Version 6.14. Bruker-AXS, Inc.: Madison, WI, 2000.

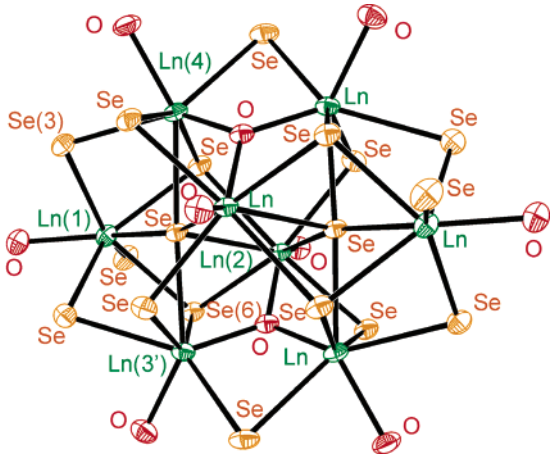

Figure 1. ORTEP diagram of the $(THF)_8Ln_8O_2Se_2(SePh)_{16}$ core, with the C and H atoms removed for clarity. Labeled atoms are mentioned in the text. Primed atoms are related to unprimed ones by inversion symmetry.

a thermoelectrically cooled InGaAs detector. The signal was intensified with a lock-in amplifier (SR 850 DSP, Stanford Research System, Sunnyvale, CA) and processed with a computer controlled by the Spectramax commercial software (GRAMS 32, Galactic Corp., Salem, NH). To measure the decay time, the laser beam was modulated at 500 Hz by a chopper and the signal was collected on a digital oscilloscope (model 54520A, 500 MHz, Hewlett-Packard, Palo Alto, CA). While these compounds lose lattice solvent quickly at room temperature, the elemental analyses indicate that coordinated solvents stay bound to the Ln over periods far longer than the time required for emission measurements.

Results

The early lanthanide benzeneselenolates reduce SeO_2 to form oxoselenido clusters (reaction 1) that crystallize as the THF adducts $(THF)_8Ln_8Se_2O_2(SePh)_{16}$ in 60−70% isolated yield (Ln = Ce (**1**), Pr (**2**), Nd (**3**), Sm (**4**)). Low-temperature structural characterization of all four compounds reveals a nearly isomorphous cluster core, with **1** and **2** crystallizing with more lattice THF than is found for **4**, and cluster **3** crystallizing in both space groups. Figure 1 shows an ORTEP diagram of the common structure for **1**−**4**, and Table 2 gives a list of significant bond geometries for **1**−**4**. The general structure consists of a hexanuclear group of Ln connected by two trigonal planar O^{2-} and two trigonal bipyramidal Se^{2-} anions. Two opposite sides of this core are capped by Ln(III) ions, and the entire group is encapsulated with 14 μ_2SePh and two terminal SePh ligands bound to the Ln that do not interact with O^{2-}. There are three distinct Ln coordination environments, with two eight coordinate central Ln (THF, O^{2-}, $2Se^{2-}$, 4μSePh), four oxo bound seven coordinate Ln (THF, O^{2-}, Se^{2-}, 4μSePh), and two seven coordinate Ln that do not interact with the oxo ligands (THF, Se^{2-}, SePh, 4μSePh). Each Ln coordinates a neutral THF donor.

$$8Ln(SePh)_3 + SeO_2 \rightarrow (THF)_8Ln_8Se_2O_2(SePh)_{16} + 8PhSeSePh + ?? \quad (1)$$

There are two structural features that distinguish the two different clusters. First is the direction of the phenyl group attached to the bridging Se atom Se(3), which, in **4**, is perpendicular to that for **1** or **2**. The Ln(1)−Se(3)−C(7)−C(8) torsion angle for **1** and **2** is −138°, and for **4** it is −40°. The subtle differences in amount of solvated THF in the lattice and the conformations of one bridging selenolate yield two different space groups and thereby two distinct crystallographic phases for the nearly isomorphic pair. Second, there is a distinctly nonlinear change in the bond length between Ln(2) and Se(6), an interaction that can arguably be described as a bond. As the lanthanide contraction progresses, average bond lengths between Ln and O^{2-}, Se^{2-}, O(THF), and SePh all decrease accordingly, with the exception of the Ln(2)−Se(6) separation, which varies from 3.39 Å (Ce) to 3.34 Å (Nd) to 3.63 Å (Sm), presumably in response to an increase in ligand−ligand repulsions as the Ln coordination spheres contract.

Thermal treatment of the Nd compound was examined to establish the identity of the solid-state phases that form upon thermal decomposition. Pyrolysis of **3** at 700 °C under vacuum gave a black solid, and X-ray powder diffraction analysis of the product indicated the presence of crystalline Nd_2Se_3,[47] $NdSe_2$,[48] and Nd_2O_3 (JCPDS 21-0579) phases (reaction 2). There was no indication of any oxoselenido phase. GCMS analysis of the volatile products identified Ph_2Se and THF in the condensate.

$$(THF)_8Ln_8Se_2O_2(SePh)_{16} \rightarrow NdSe_2 + Nd_2Se_3 + Nd_2O_3 + 8Ph_2Se + 8THF + ?? \quad (2)$$

Near-IR properties of the Nd cluster **3** and $(DME)_2Nd(SC_6F_5)_3$ (**5**) were evaluated. Absorption spectra of **3** and **5** are shown in Figure 2 with the standard spectral assignments. Most of the spectral bands in the UV−vis−NIR are well resolved with their characteristic spectral width as in other solid-state materials. The oscillator strength of the hypersensitive transition $^4I_{9/2} \rightarrow {}^4G_{5/2}$ appears to be greater in **3** relative to **5** and is smaller comparable to other reported Nd organic complexes,[49−52] and the spectrum of **3** is more complicated, as befits a compound with three chemically distinctive Nd environments. The emission spectra of **3** and **5** are compared in Figure 3, with the characteristic Nd^{3+} emission transition scheme shown in the inset. For the Nd^{3+} ion, the only excited *J* manifold that is not relaxed predominantly by multiphonon relaxation is the $^4F_{3/2}$ state. The pump photons at 800 nm populate the $^4F_{3/2}$ excited state, and relaxation to the ^4I_J (J = 9/2, 11/2, 13/2, and 15/2) manifold gives rise to the four emission bands. The observed emission wavelengths for these compounds are 927, 1078, 1360, and 1843 nm in **3** and 897, 1071, 1347, and 1824 nm in **5**. The measured fluorescence branching ratios of these transitions are in the order $^4I_{11/2} > {}^4I_{13/2} > {}^4I_{9/2} > {}^4I_{15/2}$ as is typical for Nd-based compounds.[53] In addition, numerous spectral differences can be noted between **3** and **5**. Most notably, **5** has lower emission intensity but also does not exhibit the peak splitting demonstrated by **3**.

Lifetimes of the emissions were extracted from exponential fits of the respective fluorescence decay curves (see Supporting Information). For the $^4F_{3/2} \rightarrow {}^4I_{11/2}$ emissions, the decay times

(47) Flahaut, P. J.; Guittard, M.; Patrie, M.; Pardo, M. P.; Golabi, S. M.; Domange, L. *Acta Crystallogr.* **1965**, *19*, 14.
(48) Doert, T.; Graf, C. *Anorg. Allg. Chem.* **2005**, *631*, 1101.
(49) Oczko, G. *J. Alloys Compd.* **2000**, *300*, 414.
(50) Lis, S. *J. Alloys Compd.* **2000**, *300*, 88.
(51) Gubina, K. E.; Shatrava, J. A.; Ovchynnikov, V. A.; Amirkhnov, V. M. *Polyhedron* **2000**, *19*, 2203.
(52) Legendziewicz, J.; Oczko, G.; Wiglusz, R.; Amirkhanov, V. *J. Alloys Compd.* **2001**, *323*, 792.
(53) Kaminski, A. A. *Laser Crystals-Their Physics and Properties*; Springer: Berlin, 1989.

Table 2. Average and Range of Bond Lengths [Å] and Angles [deg] for $(THF)_8Ln_8O_2Se_2(SePh)_{16}$ Phases

Ln →	Ce	Pr	Nd	Sm
Ln−O (oxide)	2.26(5)[a]/2.23−2.31	2.24(4)/2.21−2.29	2.24(4)/2.21−2.29	2.21(4)/2.18−2.25
Ln−O (THF)	2.52(2)/2.48−2.54	2.50(2)/2.47−2.53	2.49(2)/2.46−2.51	2.47(2)/2.44−2.49
Ln−Se (selenide)[b]	3.07(5)/3.04−3.15	3.05(5)/3.02−3.14	3.05(6)/3.01−3.15	3.03(6)/2.98−3.03
Ln−Se (Ph)[c]	3.08(7)/2.94−3.20	3.06(7)/2.91−3.18	3.04(7)/2.90−3.19	3.01(6)/2.89−312
Ln(2)−Se(6)	3.394	3.392	3.430	3.627
Ln−Ln[d]	3.91(4)/3.88−3.96	3.88(4)/3.85−3.92	3.86(4)/3.82−3.90	3.82(6)/3.77−3.88
<chgrow;lp;4q>Ln−Se−Ln (Se^{2-} cis)	92(9)/77−102	92(9)/77−102	93(10)/77−102	93(11)/77−104
Ln−Se−Ln (Se^{2-} trans)	168(9)/162−174	167(9)/161−174	167(9)/160−173	165(8)/159−171
Ln−Se−Ln (SePh)[e]	90(7)/78−99	89(8)/78−99	90(8)/77−100	90(9)/77−101
Ln−O−Ln (oxide)[f]	120(6)/117−124	120(4)/117−124	119(4)/117−124	119(5)/116−124
Se−Ln−O (Se^{2-}, O^{2-})	73(2)/71−75	74(2)/71−75	74(2)/72−76	75(3)/71−77

[a] The ESD of the mean is enclosed in parentheses. [b] The second Ln(2)−Se(1) bond to the 8-coordinate Ln(2) is noticeably longer at about 3.15 Å; the other selenido bonds are about 3.05 Å. [c] The longest Ln−Se bond is Ln(2)−Se(6) (~3.5 Å), so this bond is excluded from the average (see text). [d] The next closest Ln···Ln distance is Ln(1) ···Ln(4) at ~4.4 Å. [e] Angles Sm(3)′−Se(6)−Sm(2) and Sm(1)−Se(6)−Sm(2) (91.1° and 89.2°) are not included in the average. [f] For the Ln−O−Ln angles, the sum is nearly 360° indicating a planar trigonal coordination geometry of the oxide O atom, and the Ln(3)−O(1)−Ln(4) is always ~125° and the other two are always ~117°.

Table 3

host	lifetime (μs)	phonon frequency (cm^{-1})	ref
sulfide	110	450−700	77
selenide	410	450−700	77
tellurite	233−313	450−700	60
germanate	406−550	900	77
ZBLA fluoride glass	540−610	500	77
LaF_3	800	200−400	53, 58, 59
yttrium aluminum garnet	250	400	57

obtained are 186 and 111 μs, respectively, for **3** and **5**. In **3**, a decay time of 78 μs was obtained for the 925 nm emission, and in **5** a decay time of 130 μs was obtained for the 1350 nm emissions. The average decay times of the $^4F_{3/2}$ level for **3** and **5** are 55 and 60 μs, respectively. Because of the noisy signal, no decay curve was observed for the $^4F_{3/2}\rightarrow{}^4I_{15/2}$ and $^4F_{3/2}\rightarrow{}^4I_{9/2}$ transitions in **3** or the $^4F_{3/2}\rightarrow{}^4I_{13/2}$ transition in **5**. With this fluorescence decay time, the quantum yield of $^4F_{3/2}\rightarrow{}^4I_{11/2}$ emission can be estimated from the ratio of the fluorescence decay time (τ_{fl}) to radiative or "natural" decay time (τ_r). With a calculated radiative decay time of 1187 μs following the Judd−Ofelt procedure,[54,55] a quantum efficiency of 16% is obtained for **3**. In **5**, the radiative quantum efficiency obtained is 9% corresponding to a radiative decay time of 1398 μs. The effective spectral bandwidth (fwhm) of the $^4F_{3/2}\rightarrow{}^4I_{11/2}$ emission band was 38 nm in **3** and 59 nm in **5**, which is higher than that of the commercial laser glass LHG-8 (35 nm) or in Nd:YAG (30 nm).[56,57] The stimulated emission cross sections of the principal $^4F_{3/2}\rightarrow{}^4I_{11/2}$ emission bands are estimated to be 3.04×10^{-20} cm^2 for **3** and 1.61×10^{-20} cm^2 for **5**, which are comparable to the value of 1.35×10^{-20} cm^2 from the well-known host LaF_3: Nd.[58,59] The $^4F_{3/2}\rightarrow{}^4I_{13/2}$ emission band shows a spectral width of 39 nm in **3** and 31 nm in **5**, which is smaller than that of Nd-doped tellurite glass (51 nm).[60] The stimulated emission cross section of this band is estimated to be 0.30×10^{-20} cm^2, which is in the range of the reported values of Nd-doped tellurite and silicate glass.

Discussion

While lanthanide oxo cluster compounds have always held the promise of tremendous applications in both chemical and spectroscopic areas, the synthesis of such materials has always been challenging due to the tendency of LnO to react with water (reaction 3) to form hydroxide. Indeed, much of the chemistry leading to the description of crystalline oxo compounds has resulted from what is usually described as the incorporation of adventitious water into a reaction mixture. The present series of compounds is important as the first rational synthesis of hydroxy-free lanthanide clusters with oxo ligands, in reactivity that parallels the reductive generation of chalcogenido anions.

$$XLnO + HOH \leftrightarrow XLn(OH)_2 \qquad (3)$$

The selection of SeO_2 as an oxygen source is not exactly an obvious first choice reagent. In fact, the chemistry of O_2, MoO_4^{2-}, H_2O, Ph_2CO, HgO, and Ph_2CO was explored briefly before SeO_2, and while all clearly reacted with $Ln(SePh)_3$, SeO_2 was the first reactant to give a reproducible, crystalline oxo cluster product. Incorporation of both oxo and selenido ligands adds a new dimension to the Ln cluster field and is not surprising given that Se readily displaces SePh. It should be noted that analogous reactions with TeO_2 give oxo clusters without tellurido ligands, and this work is still in progress.

The geometries about the oxo ligands are at first surprising. In these materials, some of the most oxophilic metals in the periodic chart are bonding three to O^{2-} and five to Se^{2-}. Of the LnO clusters currently in the literature, there is only one with μ_3 oxo ligands, and the structure of this cluster is likely to have been influenced significantly by the steric requirements of the polydentate ancillary ligands.[26] All other Ln compounds with oxo ligands have O^{2-} with Ln_4, Ln_5, and Ln_6 coordination spheres, all in the presence of ligand systems that are viewed as classically more competitive for access to the Ln than are the ancillary SePh present here. Presumably the coordination geometry about O^{2-} in **1**−**4** is a reflection more of the physical properties of the ancillary SePh anions, which, because of their tendency to bond at right angles using selenium p orbitals, would find it increasingly difficult to bridge Ln ions that were brought closer together by higher coordinate O. With the geometry about the oxo ligands nearly trigonal planar (with Ln−O−Ln angles averaging 119.6° (**1**), 119.5° (**2**), and 119.2° (**4**)), these Ln are spaced further apart than would be Ln bound to four, five, or

(54) Judd, B. R. *Phys. Rev. B* **1962**, *127*, 750.
(55) Ofelt, G. S. *J. Chem. Phys.* **1962**, *37*, 511.
(56) Reisfeld, R.; Jorgensen, C. K. *Lasers and Excited States of Rare Earths*; Springer-Verlag: New York, 1977.
(57) Kumar, G. A.; Lu, J.; Kaminskii, A. A.; Ueda, K. I.; Yagi, H.; Yanagitani, T.; Unnikrishnan, N. V. *IEEE J. Quantum Electron.* **2004**, *40*, 747.
(58) Fan, T. Y.; Kokta, M. R. *IEEE J. Quantum Electron.* **1989**, *25*, 1845.
(59) Stouwdam, J. W.; van Veggel, F. C. J. M. V. *Nano Lett.* **2002**, *2*, 733.
(60) Shen, S.; Jha, A.; Zhang, E.; Wilson, S. J. *C. R. Chimie* **2002**, *5*, 921.

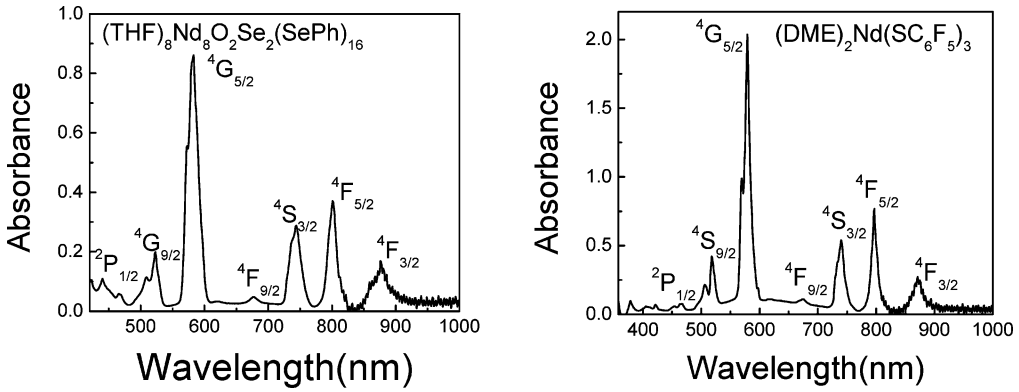

Figure 2. Absorption spectrum of $(THF)_8Nd_8O_2Se_2(SePh)_{16}$ and $(DME)_2Nd_8(SC_6F_5)_3$ measured in THF.

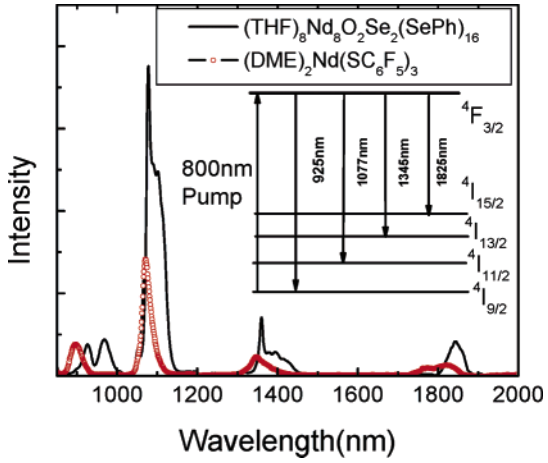

Figure 3. Comparison of the Nd^{3+} emission spectra in the two compounds with the spectroscopic schemes of the observed transitions in the inset.

six coordinate oxo ligands, and this Ln−Ln separation allows for SePh to bridge more effectively. This steric rationalization also accounts for the higher coordination at the significantly larger Se^{2-}. Alterations in structure with introduction of a stronger Lewis base solvent or the replacement of SePh with SPh/TePh will eventually prove interesting.

Thermal decomposition of the Nd cluster compound led to the observation of a series of microcrystalline Ln solid-state phases, including Nd_2O_3, Nd_2Se_3, and $NdSe_2$. There was no evidence for the formation of any ternary oxoselenido phases. Such products are not necessarily impossible synthetic targets when starting from molecular sources, but further work in both precursor design and thermolysis conditions will be required if they are to be targeted. Commercially important $Ln_2O_xE_y$ phases have been identified in the thermolysis of $(THF)_6Ln_4S_9I_2$, but only when the displaced THF was not trapped immediately upon dissociation.[61] Clearly, reaction conditions and precursor identities will have to be examined systematically if single-phase oxochalcogenido solids are to be approached from molecular sources.

The near-IR emission properties of the Nd cluster **3** and thiolate **5** are consistent with Nd ions bound to heavier S- and Se-based anions. All of the absorption and emission bands in **3** show considerable red shift that is attributed to the higher nephelauxetic effect in **3** due to the increased covalency and ligand coordination.[62] The emission spectra of **3** and **5** are different in terms of the Stark level splitting, broadening, and the intensity, and all of these depend on the coordination environment of the emitting Nd ion and the number of Nd ions in the compound. Compound **5** shows less emission intensity and quantum efficiency mainly due to the lower ionic concentration (1.26×10^{21} Nd ions/cc in **5** and 1.92×10^{21} Nd ions/cc in **3**) and consequent energy transfer quenching. The reported 111−186 μs emission lifetimes are typical of low phonon energy hosts, where the emission lifetimes of various classes of low phonon energy hosts are found to range from 100 to 800 μs (Table 3). The calculated radiative lifetimes are comparable to the reported values in organic compounds,[63] whereas the fluorescence decay time of 186 μs and 16% quantum yield are considered to be the highest reported values among Nd organic complexes. Earlier, Hasegawa et al. obtained a decay time of 13 μs and a quantum yield of 3.2% in Nd(bis-perfluorooctanesulfonylimide)$_3$,[64] and in all other reports[65−71] the quantum yields obtained are in the range of 10^{-2}−10^{-5}.

In addition to concentration quenching, the major factors reducing the fluorescence quantum yield in Nd systems are multiphonon relaxation of the ceramic cluster core and vibrational quenching by nearby organic ligands. For Nd^{3+} ions, one principal channel for nonradiative multiphonon relaxation is through $^4F_{3/2} \rightarrow {}^4I_{15/2}$, which is emission at 1843 nm. The energy gap of this band in the present Nd complexes is 5868 cm^{-1}, and, assuming the highest vibrational frequencies of Nd−O and Nd−Se are ca. 700 and 400 cm^{-1}, respectively,[72] 8 and 15 phonons are required to bridge the $^4F_{3/2} \leftrightarrow {}^4I_{15/2}$ energy gap. The

(61) Melman, J. H. Ph.D. Thesis, Rutgers University. UMI, Order No. DA3117623 (2004). From: *Diss. Abstr. Int., B* **2004**, *64*, 6084.

(62) Jorgenson, C. K. *Modern aspects of Ligand Filed Theory*; North Holland: Amsterdam, 1971.
(63) Hasegawa, Y.; Murakoshi, K.; Wada, Y.; Kim, J. H.; Nakashima, N.; Yamanaka, T.; Yanagida, S. *Chem. Phys. Lett.* **1996**, *260*, 173.
(64) Hasegawa, H.; Okhubo, T.; Sogabe, K.; Kawamura, Y.; Wada, Y.; Nakashima, N.; Yanagida, S. *Angew. Chem., Int. Ed.* **2000**, *39*, 357.
(65) Slooff, L. H.; Polman, A.; Klink, S. I.; Hebbink, G. A.; Grave, L.; van Veggel, F. C. J. M.; Reinhoudt, D. N.; Hofstraat, J. W. *Opt. Mater.* **2000**, *14*, 101.
(66) Wolbers, M. P. O.; van Veggel, F. C. J. M.; Hofstraat, J. W.; Geurts, F. A. J.; Reinhoudt, D. N. *J. Chem. Soc., Perkin Trans.* **1997**, 2275.
(67) Wolbers, M. P. O.; van Veggel, F. C. J. M.; Snellink-Ruel, B. H. M.; Hofstraat, J. W.; Geurts, F. A. J.; Reinhoudt, D. N. *J. Chem. Soc., Perkin Trans.* **1998**, 2141.
(68) Klink, S. I.; Hebbink, G. A.; Grave, L.; van Veggel, F. C. J. M.; Reinhoudt, D. N.; Slooff, L. H.; Polman, A.; Hofstraat, J. W. *J. Appl. Phys.* **1999**, *86*, 1181.
(69) Hebbink, G. A.; van Veggel, F. C. J. M.; Reinhoudt, D. N. *Eur. J. Org. Chem.* **2001**, 4101.
(70) Hasegawa, Y; Murakoshi, K.; Wada, Y.; Kim, J. H.; Nakashima, N.; Yamanaka, T.; Yanagida, S. *Chem. Phys. Lett.* **1996**, *248*, 8.
(71) Wada, Y.; Okubo, T.; Ryo, M.; Nakazawa, T.; Hasegawa, Y.; Yanagida, S. *J. Am. Chem. Soc.* **2000**, *122*, 8583.
(72) Berg, D. J.; Burns, C. J.; Andersen, R. A.; Zalkin, A. *Organometallics* **1989**, *8*, 1865.

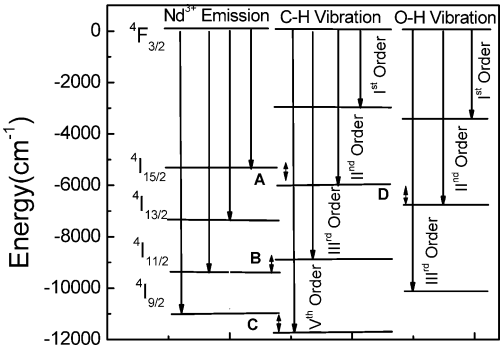

Figure 4. Schematic representation of the vibrational quenching of the $^4F_{3/2}$ emission in Nd^{3+} by the vibrational modes of CH and OH functional groups. The energy differences between the interacting levels of Nd^{3+} and the vibrational groups are labeled with A, B, C, and D where $\Delta E_A = 489$ cm^{-1}, $\Delta E_B = 435$ cm^{-1}, $\Delta E_C = 565$ cm^{-1}, and $\Delta E_D = 1432$ cm^{-1}.

probability of such a high order process is limited, and the result is that the $^4F_{3/2} \rightarrow {}^4I_{15/2}$ transition is radiative, contrary to other high phonon energy hosts where the band at 1843 nm could not be observed. It seems reasonable to assume that the multitude of SePh ligands have detracted from optimal quantum efficiency. Elimination of SePh ligands will presumably improve quantum efficiency, and experiments along those lines are in progress.

The fluorescence quenching mechanism of various Nd^{3+} emission bands by the presence of OH (3450 cm^{-1}) and CH (2950 cm^{-1}) vibration is schematically shown in Figure 4. The second-, third-, and fourth-order CH bond vibrational frequencies are almost in resonance (energy difference is of the order of 435−565 cm^{-1}) with the emission bands at 1825 ($^4F_{3/2} \rightarrow {}^4I_{15/2}$), 1077 ($^4F_{3/2} \rightarrow {}^4I_{11/2}$), and 890 nm ($^4F_{3/2} \rightarrow {}^4I_{9/2}$), and hence there are chances of energy transfer by the Forster mechanism,[73] the extent of which depends directly on the overlap of the emission spectrum of Nd with the absorption spectrum of OH/CH and inversely on the sixth power of the separation between Nd and vibrating species. Quenching due to OH overtones primarily influences the $^4F_{3/2} \rightarrow {}^4I_{13/2}$ band. Our detailed energy transfer simulation[74] shows that in both molecules **3** and **5** there is strong fluorescence quenching (84% in **3** and 91% in **5**) and the major sources of this quenching are (1) concentration quenching due to multipolar energy transfer interactions between Nd ions and (2) the presence of CH bonds. In both complexes, the Nd−Nd separation is always less than that of Nd−CH, and hence the major contribution of the fluorescence quenching comes from the interaction between Nd ions.

In the present compounds, O−H is completely absent, and C−H is present, but in an apparently limited sense. In the fluorinated thiolate, C−H units are found only on the DME ligand that coordinates weakly though Nd−OR_2 bonds. In cluster **3**, there are C−H bonds in the weakly bound THF ligand and in the Ph (Se) ligands encapsulating the cluster core. The SePh are also considered to be weakly bound to the Ln, and these ligands are distanced by the relatively long Nd−Se bond lengths. It seems reasonable to assume that the multitude of SePh ligands have detracted from optimal quantum efficiency. With direct coordination of Nd^{3+} to heavier atoms, the coupling between the energy levels is less efficient and the Franck−Condon factor for the relaxation process is reduced, effectively increasing the lifetime. Thus, for this reason, both compounds are more emissive in the near-IR spectrum, particularly when compared to the current literature.

Absolute relationships that correlate structure and quantum efficiencies (QE) are still elusive. For Er, both the molecular thiolate $(DME)_2Er(SC_6F_5)_3$[75] and the decanuclear cluster $(THF)_8Er_{10}S_6Se_{12}I_6$ were found to be similarly emissive (QE = 78% and 75%, respectively), while QE dropped dramatically in heterometallic $(py)_8M_2Er_4Se_6(SePh)_4$ (M = Cd, Hg).[76] In the present Nd experiments, the fluorinated thiolate compound **5** is shown to be the most emissive monometallic Nd compound reported to date, and cluster **3**, with a significant number of hydrocarbon functionalized selenolate ligands, has even brighter emission properties, with the highest quantum efficiency reported for a discrete Nd compound, and a high concentration of Nd ions that should be useful when doping into apolar matrixes. Further developments in the areas of oxo and non-oxo clusters are currently under investigation.

Conclusions

Oxo ligands are readily introduced into lanthanide cluster chemistry by the reduction of SeO_2 with $Ln(SePh)_3$. The relatively strong Ln−O bond does not negatively impact Ln emission properties. The investigation into the emission properties of the molecular thiolate compound $(DME)_2Nd(SC_6F_5)_3$ and the oxyselenido cluster $(THF)_8Nd_8O_2Se_2(SePh)_{16}$ reveals emission at 925 and 1077 nm. Furthermore, for the first time, emission at 1.35 and 1.83 μm has been observed from a molecular Nd(III) source.

Acknowledgment. This work was supported by the National Science Foundation under Grant No. CHE-0303075, and the APEX diffractometer was obtained under Grant No. CHE-0091872. Support from the New Jersey State Commission on Science and Technology is gratefully acknowledged by R.E.R.

Supporting Information Available: X-ray crystallographic files in CIF format for the crystal structures of **1**−**4**. Fluorescence decay curves and exponential fits. This material is available free of charge via the Internet at http://pubs.acs.org.

JA054261Q

(73) Forster, T. *Ann. Phys.* **1948**, *2*, 55.
(74) Kumar, G. A.; Riman, R. E.; Diaz-Torres, L. A.; Banerjee, S.; Romanelli, M.; Brennan, J. G., manuscript in preparation.
(75) Kumar, G. A.; Riman, R. E.; Banerjee, S.; Kornienko, A.; Brennan, J. G. *Chem. Mater.* **2005**, *17*, 5130.
(76) Kornienko, A.; Banerjee, S.; Kumar, G. A.; Riman, R.; Emge, T. J.; Brennan, J. G. *J. Am. Chem. Soc.* **2005**, *127*, 14008.
(77) *Optical Fiber Amplifiers-Materials, Devices, and Applications*; Sudo, S., Ed.; Artech House Inc.: Norwood, MA, 1997.